**PHYSICS AND CHEMISTRY OF SOLID STATE**
V. 26, No.4 (2025) pp. 833-843
*Section: Chemistry*

**DOI: 10.15330/pcss.26.4.833-843**

*Vasyl Stefanyk Carpathian National University*

**ФІЗИКА І ХІМІЯ ТВЕРДОГО ТІЛА**
**Т. 26, № 4 (2025) С. 833-843**
*Хімічні науки*

PACS: 71.15.Mb

ISSN 1729-4428
(Print)
ISSN 2309-8589 (Online)

Fatemeh Mollaamin

# Nano-based Materials for Environmental Soil Remediation due to Noxious Transition Metals Removal: Structural, Electromagnetic and Thermodynamic Analysis by DFT Outlook

*Department of Biomedical Engineering, Faculty of Engineering and Architecture, Kastamonu University, Kastamonu, Turkey, fmollaamin@kastamonu.edu.tr*

The target of this research is removing transition metals of Cr, Mn, Fe, Zn, W, Cd from soil due to nanomaterial-based gallium nitride nanocage ($B_5N_{10}$-nc). The electromagnetic and thermodynamic attributes of toxic transition metals trapped in $B_5N_{10}$-nc were depicted by materials modeling. It has been studied the behavior of trapping of Cr, Mn, Fe, Zn, W, Cd by $B_5N_{10}$-nc for sensing the soil metal cations. $B_5N_{10}$-nc was designed in the existence of transition metals (Cr, Mn, Fe, Zn, W, Cd). Case characterization was performed by DFT method. The nature of covalent features for these complexes has represented the analogous energy amount and vision of the partial density of states between the *p* states of boron and nitrogen in $B_5N_{10}$-nc with and *d* states of Cr, Mn, Fe, Zn, W, Cd in X↔ $B_5N_{10}$-nc complexes. Furthermore, the nuclear magnetic resonance (NMR) analysis indicated the notable peaks surrounding Cr, Mn, Fe, Zn, W, Cd through the trapping in the $B_5N_{10}$-nc during atom detection and removal from soil; however, some fluctuations can be observed in the chemical shielding treatment of isotropic and anisotropy tensors. Based on the results in this research, the selectivity of toxic metal, metalloid and nonmetal elements adsorption by $B_5N_{10}$-nc (atom sensor) have been indicated as: Cd> Zn> Fe> Cr> Mn ≈ W. In this article, it is proposed that toxic metal, metalloid and nonmetal elements–adsorbed might be applied to design and expand the optoelectronic specifications of $B_5N_{10}$-nc for generating photoelectric instruments toward soil purification.

**Keywords:** Soil contamination; $B_5N_{10}$-nc; molecular modeling; nanomaterial; DFT.

*Received 17 January 2025; Accepted 27 November 2025.*

## Introduction

Geogenic processes and anthropogenic activities are two important sources of soil pollution. Soils may inherit toxic metals from parent materials; however, soil pollution mostly results from industrial and agricultural activities. Contamination by metals can be indicated by the changes in chemical, biochemical, and microbial properties of soils and plant responses. The total concentration of toxic metals in soil is still the most widely used indicator for risk assessment although extractable amounts have been reported to be more closely related to plant uptake. Heavy metals remark to some metals and metalloids having biological toxicity like Cd, Hg, As, Pb, and Cr [1]. Heavy metal contamination of soil and the environment have been accelerated in modern society due to industrialization, rapidly expanded world population, and intensified agriculture. Accumulation of heavy metals often results in soil/water degradation and ecosystem malfunction. Moreover, heavy metals enter food chains from polluted soil, water, and air, and consequently cause food contamination, thus posing a threat to human and animal health [2].

Trace metals in soils and dusts can be accumulated in the human body via direct inhalation, ingestion, and dermal contact absorption [3] or via the soil-crop system [4]. The anthropogenic sources of metals include traffic emission, industrial and domestic emission, atmospheric deposition, mining, waste disposal, sewage, pesticides, and fertilizers [5]. Without proper management,

abandoned mines will cause more serious environmental impacts compared with active mines [6]. Consumption of food crops growing in contaminated area is one of the important sources of human exposure to metals in mining areas [7].

Soil contamination in urban environment by trace metals is of public concerns. For better risk assessment, it is important to determine their background concentrations in urban soils. For instance, Molybdenum (Mo) is an essential trace element for human, animal, and plant health. Mo deficiency in soils has frequently been reported, especially under P-deficient conditions. However, Mo is also a potentially toxic contaminant to soils and aquifers that may pose significant threat to ecological and human health [8].

Another research studied the sources and extent of arsenic (As) contamination and the translocation and speciation from microbes to soil are illustrated [9].

Moreover, several activities can build up soil copper (Cu) concentrations leading to incorporation into the food chain and adversely affect natural and managed ecosystems [10].

The cobalt (Co)-contaminated soil has exposed potential toxicity to humans, plants, and animals. Recently, scientists have summarized the natural and anthropogenic sources arousing the increase of cobalt in soil and reviewed the cobalt species in soil and factors that influence the mobilization of cobalt [11].

Soil contamination in urban environment by trace metals is of public concerns. For better risk assessment, it is important to determine their background concentrations in urban soils. One investigation determined the concentrations of 9 trace metals including As, Ba, Cd, Co, Cu, Ni, Pb, Se, and Zn in 214 urban soils from 6 cities of different sizes from both public and commercial sites in Florida [12].

Remediation using chemical, physical, and biological methods have been adopted to solve the problem. Up to date, phytoremediation approach has affirmed to be a promising viewpoint to traditional methods as it is environmentally friendly, cost effective. Boron nitride nanomaterials have been used owing to their unique characteristics such as eco-friendly attributes for pollutant adsorption, big surface area, high chemical & mechanical strength and semiconducting property [13].

Boron nitride nanometerials usually exhibit semi-leading behavior, which is considered a proper alternative to carbon nanotubes. The properties of boron and nitrogen atoms which are the first neighbors of carbon in the periodic table, make boron nitride as an interesting subject of numerous studies [14].

In recent years, different investigations on the adsorption of chemical contaminants and applying various boron nitride nanomaterials as adsorbents for water purification have been studied [15].

Various physical shapes of boron nitride (BN)-based nano adsorbents such as nanoparticles, fullerenes, nanotubes, nanofibers, nanoribbons, nanosheets, nanomeshes, nanoflowers, and hollow spheres have been broadly considered possible adsorbents owing to their exceptional characteristics such as large surface area, structural variability, great chemical/mechanical strength, abundant structural defects, high reactive sites, and functional groups.

In this work, $B_5N_{10}$-nc has been modeled for trapping transition metals of Cr, Mn, Fe, Zn, W, Cd. Physical and chemical properties of the interaction binding between Cr, Mn, Fe, Zn, W, Cd, and boron/ nitrogen in $B_5N_{10}$-nc have been estimated.

# I. Theory, substances, and approaches

### 1.1. Trapping metal, metalloid and nonmetal elements in $B_5N_{10}$-nc

The goal of this research article is to detect and trap the metal, metalloid and nonmetal atoms from soil by using $B_5N_{10}$-nc. The intention is to remove Cr, Mn, Fe, Zn, W, Cd from the soil medium containing toxic ingredients. The soil medium consists of metal, metalloid and nonmetal atoms and the added $B_5N_{10}$-nc (Figure1a–f). $B_5N_{10}$-nc was modeled in the presence of Cr, Mn, Fe, Zn, W, Cd through computational methods of density functional method of *CAM–B3LYP–D3.*

The metal, metalloid and nonmetal atoms were successfully incorporated in the center of $B_5N_{10}$-nc toward formation of Cr↔$B_5N_{10}$-nc, Mn↔$B_5N_{10}$-nc, Fe↔$B_5N_{10}$-nc, Zn↔$B_5N_{10}$-nc, W↔$B_5N_{10}$-nc, and Cd↔$B_5N_{10}$-nc complexes (Figure1a–f) and charge distribution of these complexes has been computed owing to the parameter of Bader charge evaluation [16]. Irrespective of what element, the $B_5N_{10}$-nc becomes bigger for embedding these elements.

### 1.2. Method of Density functional theory (DFT)

There are many ions and electrons in a metallic solid which form a many-body system. DFT has been performed in this article due to projector / ameliorated / wave method, Perdew / Burke / Ernzerhof functional based on the generalized gradient approximation as the exchange-correlation functional, and non-empirical PBE functional [17].

For years, metals and metalloids with computed bandwidths have been an important discussion through DFT. In this paper, it has been investigated first principles calculations for trapping transition metals of Cr, Mn, Fe, Zn, W, Cd by $B_5N_{10}$-nc using DFT methods.

The electronic density within the Kohn-Sham (KS) equations leads us to a considerable reduction in quantum computing towards Hamiltonian parameter [18]:

$$\widehat{H}_s = -\sum_i^M \frac{1}{2} \overline{\nabla}_i^2 + \sum_i^M v_s(\vec{r}_i) = \sum_i^M \hat{h}_s;$$

$$\hat{h}_s = -\frac{1}{2} \overline{\nabla}_i^2 + v_s(\vec{r}_i), \quad (1)$$

where $M$ is non-interactive electrons, $v_s$ is external potential. Thus, by measuring $\psi_i$ (single particle orbitals), the parameter of electronic densities for electrons with noninteractions will be:

$$\rho(\vec{r}) = \sum_i^M |\psi_i(\vec{r})|^2 \quad (2)$$

So, the total energy will be:

$$E[\rho] = \sum_i^M n_i \langle \psi_i \left| -\frac{1}{2}\bar{\nabla}^2 + v_{ext}(\vec{r}) + \frac{1}{2}\int \frac{\rho(\vec{r}')}{|\vec{r}-\vec{r}'|}\, d\vec{r}' \right| \psi_i \rangle + E_{xc}[\rho] + \frac{1}{2}\sum_\beta^N \sum_{\alpha\neq\beta}^N \frac{Z_\alpha Z_\beta}{|\vec{R}_\alpha - \vec{R}_\beta|} \quad (3)$$

Furthermore, B3LYP (Becke, Lee, Yang, Parr) function as a hybrid functional of 3-parameter basis function and LANL2DZ basis set for metals and metalloids within DFT approach [19]. In addition, a new hybrid exchange–correlation functional called CAM–B3LYP was suggested which merges B3LYP and the long-range correction [20]. Moreover, the DFT functionals with Grimme's D3 correction have been considered [21]. The approach of dispersion correction is added to Kohn-Sham density functional theory (DFT-D) with higher accuracy [22].

In this work, DFT computations were accomplished by Gaussian 16 revision C.01 program package [23]. The z-matrix coordination has been built for trapping transition metals of Cr, Mn, Fe, Zn, W, Cd in soil by the $B_5N_{10}$-nc using GaussView 6.1 [24] via the solid model and coordination (Figure2 a–f).

The consequences will remark on the following challenges faced by the DFT approaches in accurately describing the (transition metals) - (boron and nitrogen) bonding.

## II. Results and Discussions

$B_5N_{10}$-nc has been modeled for trapping transition metals of Cr, Mn, Fe, Zn, W, Cd. Physical and chemical properties of the interaction binding between Cr, Mn, Fe, Zn, W, Cd, and boron/ nitrogen in $B_5N_{10}$-nc have been estimated.

### 2.1. Electronic Evaluation & PDOS

The electronic structure of toxic element trapping including Cr, Mn, Fe, Zn, W, Cd using $B_5N_{10}$-nc has been illustrated using *CAM–B3LYP–D3/*6–311+G (d,p), *LANL2DZ* level of theory.

Figure 3 (a–f) shows the projected density of state (PDOS) of X↔$B_5N_{10}$-nc through Cr, Mn, Fe, Zn, W, Cd encapsulation. The existence of the energy states (*p*-orbital) of B, N, and (*d*-orbital) of Cr, Mn, Fe, Zn, W, Cd within the gap of X↔$B_5N_{10}$-nc induces the reactivity of the system. It is clear from the figure that after trapping of

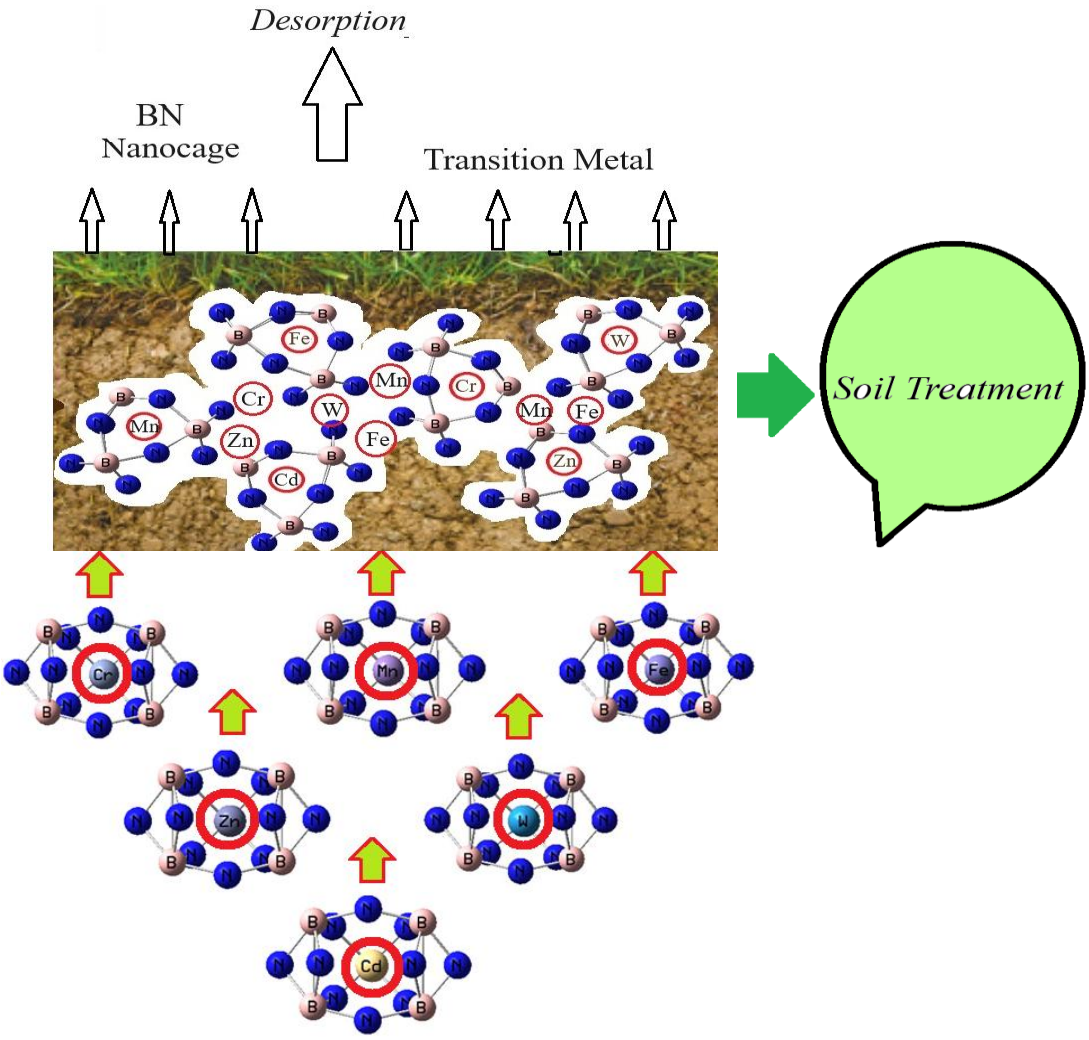


**Fig. 1.** Trapping of some contaminant elements of Cr, Mn, Fe, Zn, W, Cd in polluted soil via $B_5N_{10}$-nc and formation of Cr↔$B_5N_{10}$-nc, Mn↔$B_5N_{10}$-nc, Fe↔$B_5N_{10}$-nc, Zn↔$B_5N_{10}$-nc, W↔$B_5N_{10}$-nc, and Cd↔$B_5N_{10}$-nc complexes toward clean soil.

transitions metals, there is a significant contribution of *d*-orbital in the unoccupied level. Therefore, the curve of partial PDOS has described that *p* states of B, N atoms in $B_5N_{10}$-nc and *d*-orbital of Cr, Mn, Fe, Zn, W, Cd in X↔$B_5N_{10}$-nc overcome due to the conduction band (Figure 3a–f). A distinguished adsorption trait might be seen in X↔$B_5N_{10}$-nc because of the potent interaction between the *p* states of boron and nitrogen in $B_5N_{10}$-nc with *d* states of As, Se, Co, Cu, Mo in X↔$B_5N_{10}$-nc complexes.

Figure 3(a–f) shows that Cr↔$B_5N_{10}$-nc, Mn↔$B_5N_{10}$-nc, Fe↔$B_5N_{10}$-nc, Zn↔$B_5N_{10}$-nc,

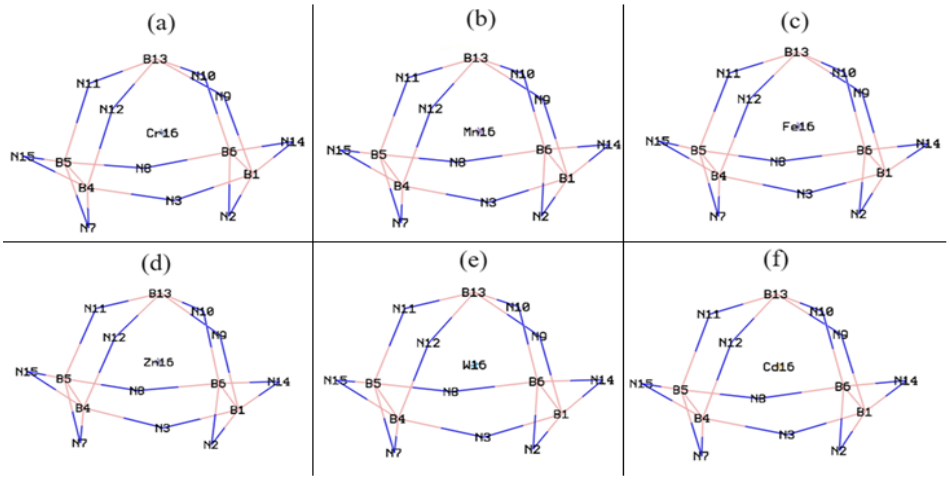


**Fig. 2.** Optimized complexes of a) Cr↔$B_5N_{10}$-nc, b) Mn↔$B_5N_{10}$-nc, c) Fe↔$B_5N_{10}$-nc, d) Zn↔$B_5N_{10}$-nc, e) W↔$B_5N_{10}$-nc, and f) Cd↔$B_5N_{10}$-nc using CAM–B3LYP–D3/EPR–3, LANL2DZ.

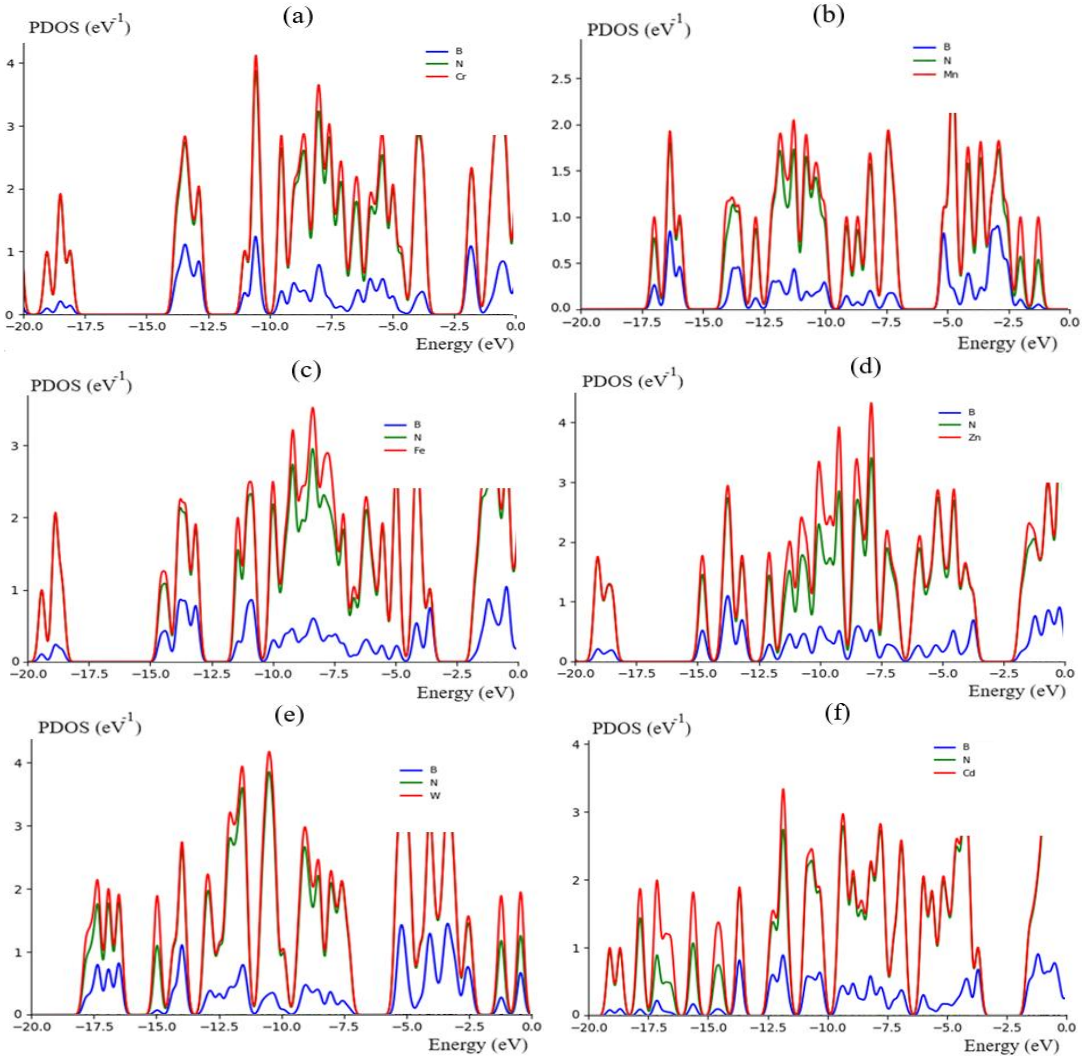


**Fig. 3**. PDOS encapsulation of transition metals by $B_5N_{10}$-nc toward formation of complexes including a) Cr↔$B_5N_{10}$-nc, b) Mn↔$B_5N_{10}$-nc, c) Fe↔$B_5N_{10}$-nc, d) Zn↔$B_5N_{10}$-nc, e) W↔$B_5N_{10}$-nc, and f) Cd↔$B_5N_{10}$-nc by *CAM–B3LYP–D3/*6–311+G (d,p*)*, LANL2DZ.

W↔$B_5N_{10}$-nc, and Cd↔$B_5N_{10}$-nc complexes have the most contribution at the middle of the conduction band between –5 to –15 eV, while contribution of boron and nitrogen states are enlarged and similar together, and grabbing of Cr, Mn, Fe, Zn, W, Cd depicts interfacial electronic of the $B_5N_{10}$-nc for selection of these atoms. Cr ↔$B_5N_{10}$-nc has indicated one sharp peak around –10 eV for Cr in Figure 3 (a), while Mn↔$B_5N_{10}$-nc (Figure3b) has a sharp peak around –5 eV for Mn. The complexes of Fe↔$B_5N_{10}$-nc (Figure3c) and Zn↔$B_5N_{10}$-nc (Figure3d) have exhibited a sharp peak around –8.5 eV for Fe and Zn atoms, respectively. Furthermore, W↔$B_5N_{10}$-nc (Figure3e) has exhibited a strong peak around –10 eV through the graphs for W. Moreover, Cd graph in Cd↔$B_5N_{10}$-nc (Figure3f) with a sharp peak around –12.5 eV attracts our attention.

As it can be seen, the order potency of atom grabbing of Cr, Mn, Fe, Zn, W, Cd by $B_5N_{10}$-nc based on the PDOS might be shifted as:
Cd ↔ $B_5N_{10}$-nc > W ↔ $B_5N_{10}$-nc ≈ C↔$B_5N_{10}$-nc > Zn↔$B_5N_{10}$-nc ≈Fe↔$B_5N_{10}$-nc >> Mn↔$B_5N_{10}$-nc.

### 2.2. Theoretical Insight & Analysis of electric potential

Nuclear quadrupole is a resonance (NQR) related to NMR which shows the unsymmetrical distribution of electric charge of a spinning nucleus. All nuclei with a spin number 1 > 1 have a magnetic moment and an electric quadrupole moment that measures the deviation of the distribution of the positive charge in the nucleus [25].

In this work, the quantum mechanics of NQR at zero-field containing the magnitudes of nuclear quadrupole moments have been carried out on trapping Cr, Mn, Fe, Zn, W, Cd by $B_5N_{10}$-nc [26]:

$$V(r) = V(0) + \left[\left(\frac{\partial V}{\partial x_i}\right)\Big|_0 . x_i\right] + \frac{1}{2}\left[\left(\frac{\partial^2 V}{\partial x_i x_j}\right)\Big|_0 . x_i x_j\right] + \cdots \quad (4)$$

$$U = -\frac{1}{2}\int_{\mathcal{D}} d^3\, r\, \rho_r \left[\left(\frac{\partial^2 V}{\partial x_i^2}\right)\Big|_0 . x_i^2\right] = -\frac{1}{2}\int_{\mathcal{D}} d^3\, r\, \rho_r \left[\left(\frac{\partial E_i}{\partial x_i}\right)\Big|_0 . x_i^2\right] = -\frac{1}{2}\left(\frac{\partial E_i}{\partial x_i}\right)\Big|_0 . \int_{\mathcal{D}} d^3\, r\, [\rho(r) . x_i^2] \quad (5)$$

$$\chi = {e^2 Q q_{zz}}/{h} \quad (6)$$

$$\eta = {q_{xx} - q_{yy}}/{q_{zz}} \quad (7)$$

Since the electric field gradient (EFG) at the settlement of the nucleus in metal, metalloid and nonmetal atoms including Cr, Mn, Fe, Zn, W, Cd is defined by the valence electrons bent in the pure location with familiar nuclei of $B_5N_{10}$-nc through trapping of Cr, Mn, Fe, Zn, W, Cd, the frequency of NQR at which intermediates occur is only for X↔$B_5N_{10}$-nc complexes (X = Cr, Mn, Fe, Zn, W, Cd) (Table1). In the present research, the electric potential via Bader charge was estimated for Cr↔$B_5N_{10}$-nc, Mn↔$B_5N_{10}$-nc, Fe↔$B_5N_{10}$-nc, Zn↔$B_5N_{10}$-nc, W↔$B_5N_{10}$-nc, and Cd↔$B_5N_{10}$-nc complexes (Table1).

Furthermore, in Figure4 (a–f), the graph of electric potential fluctuation via Bader charge for toxic transition metals of Cr, Mn, Fe, Zn, W, Cd grabbed by the $B_5N_{10}$-nc have been assessed.

In Figure4 (a–f), the trapping fluctuation of Cr, Mn, Fe, Zn, W, Cd by $B_5N_{10}$-nc for sensing the toxic metal, metalloid and nonmetal atoms in the contaminated soil can be observed. The graph of $B_5N_{10}$-nc is bent by these toxic atoms. The sharpest curves for electric potential were nominated for metal, metalloid and nonmetal atoms trapped by the $B_5N_{10}$-nc that prove the electron attaining of these element aided by boron and nitrogen atoms of $B_5N_{10}$-nc based on the relation coefficient of $R^2$ as:
Cd ↔ $B_5N_{10}$-nc>Zn ↔ $B_5N_{10}$-nc ≈
≈Cr↔$B_5N_{10}$-nc>Fe↔$B_5N_{10}$-nc>Mn↔$B_5N_{10}$-nc
>W↔$B_5N_{10}$-nc (Figure4a–f).

### 2.3. Background & Application of Nuclear Magnetic Resonance (NMR)

The investigation of NMR of high- materials and other correlated-electron systems improved for conventional superconductors and d-band transition metals, alloys, and intermetallic compounds [27].

As a matter of fact, magnetic field gradients fix it feasible to tag spatial coordinates within a model. The frequencies resonance of most atoms is well segregated from each other which causes NMR to be an element-specific method. Interactions of spins with their local environment direct to spectral alterations that evoke the local geometry and physico-chemical states. Therefore, NMR spectrum of $B_5N_{10}$-nc for trapping metal, metalloid and nonmetal atoms containing Cr, Mn, Fe, Zn, W, Cd might illustrate the possibility of $B_5N_{10}$-nc for sensing and grabbing of these toxic elements from contaminated soil toward measuring the isotropic chemical-shielding (CSI) and anisotropic chemical-shielding (CSA) [28]:

$$\sigma_{iso} = (\sigma_{11} + \sigma_{22} + \sigma_{33})/3; \quad (8)$$

$$\sigma_{aniso} = \sigma_{33} - (\sigma_{22} + \sigma_{11})/2 \quad (9)$$

The NMR quantities of isotropic ($\sigma_{iso}$) and anisotropic shielding tensor ($\sigma_{aniso}$) of Ba, As, Se, Co, Cu, Mo trapped on the in the $B_5N_{10}$-nc towards formation of Cr↔$B_5N_{10}$-nc, Mn↔$B_5N_{10}$-nc, Fe↔$B_5N_{10}$-nc, Zn↔$B_5N_{10}$-nc, W↔$B_5N_{10}$-nc, and Cd↔$B_5N_{10}$-nc complexes was computed by Gaussian 16 revision C.01 program package (Table2).

Table 2 has reported NMR amounts for transition metals of Cr, Mn, Fe, Zn, W, Cd encapsulated in the $B_5N_{10}$-nc. Grabbing Cr, Mn, Fe, Zn, W, Cd shows the spin polarization on the (Cr, Mn, Fe, Zn, W, Cd)–encapsulated $B_5N_{10}$-nc. The increase in the chemical shift anisotropy spans for atom trapping by the $B_5N_{10}$-nc are near N (2), N (3), N (7), N (8), N (9), N (10), N (11), N (12), N (14) and N (15) (Table2). The observed weak signal intensity near the parallel edge of the nanocage might be owing to boron binding induced non-spherical distribution of these

**Table 1.**

The amounts of electric potential ($E_p$ /a.u.) and Bader charge (Q /coulomb) through NQR calculation for Cr↔$B_5N_{10}$-nc, Mn↔$B_5N_{10}$-nc, Fe↔$B_5N_{10}$-nc, Zn↔$B_5N_{10}$-nc, W↔$B_5N_{10}$-nc, and Cd↔$B_5N_{10}$-nc complexes.

| Cr↔$B_5N_{10}$-nc | | | Mn↔$B_5N_{10}$-nc | | | Fe↔$B_5N_{10}$-nc | | |
|---|---|---|---|---|---|---|---|---|
| Atom | Q | $E_p$ | Atom | Q | $E_p$ | Atom | Q | $E_p$ |
| B1 | 0.282 | –11.239 | B1 | 0.188 | –11.219 | B1 | 0.271 | –11.244 |
| N2 | –0.205 | –18.105 | N2 | –0.052 | –18.282 | N2 | –0.184 | –18.089 |
| N3 | –0.254 | –18.116 | N3 | –0.165 | –18.305 | N3 | –0.251 | –18.114 |
| B4 | 0.330 | –11.232 | B4 | 0.201 | –11.216 | B4 | 0.314 | –11.247 |
| B5 | 0.320 | –11.241 | B5 | 0.227 | –11.211 | B5 | 0.313 | –11.242 |
| B6 | 0.319 | –11.222 | B6 | 0.199 | –11.214 | B6 | 0.278 | –11.245 |
| N7 | –0.198 | –18.117 | N7 | –0.055 | –18.283 | N7 | –0.174 | –18.100 |
| N8 | –0.269 | –18.126 | N8 | –0.164 | –18.294 | N8 | –0.243 | –18.109 |
| N9 | –0.338 | –18.141 | N9 | –0.051 | –18.295 | N9 | –0.364 | –18.145 |
| N10 | –0.312 | –18.135 | N10 | –0.057 | –18.291 | N10 | –0.319 | –18.140 |
| N11 | –0.288 | –18.145 | N11 | –0.070 | –18.289 | N11 | –0.277 | –18.131 |
| N12 | –0.365 | –18.128 | N12 | –0.080 | –18.297 | N12 | –0.398 | –18.132 |
| B13 | 0.110 | –11.245 | B13 | 0.304 | –11.219 | B13 | –0.021 | –11.270 |
| N14 | –0.162 | –18.096 | N14 | –0.115 | –18.294 | N14 | –0.136 | –18.079 |
| N15 | –0.170 | –18.112 | N15 | –0.138 | –18.293 | N15 | –0.159 | –18.097 |
| Cr16 | 1.201 | –101.752 | Mn16 | –0.172 | –16.560 | Fe16 | 1.352 | –113.900 |
| Zn↔$B_5N_{10}$-nc | | | W↔$B_5N_{10}$-nc | | | Cd↔$B_5N_{10}$-nc | | |
| Atom | Q | $E_p$ | Atom | Q | $E_p$ | Atom | Q | $E_p$ |
| B1 | 0.280 | –11.252 | B1 | 0.201 | –11.220 | B1 | 0.277 | –11.244 |
| N2 | –0.229 | –18.124 | N2 | –0.076 | –18.292 | N2 | –0.246 | –18.137 |
| N3 | –0.213 | –18.101 | N3 | –0.208 | –18.308 | N3 | –0.223 | –18.097 |
| B4 | 0.323 | –11.245 | B4 | 0.229 | –11.212 | B4 | 0.323 | –11.238 |
| B5 | 0.317 | –11.246 | B5 | 0.254 | –11.209 | B5 | 0.301 | –11.251 |
| B6 | 0.298 | –11.245 | B6 | 0.232 | –11.212 | B6 | 0.294 | –11.243 |
| N7 | –0.194 | –18.112 | N7 | –0.046 | –18.293 | N7 | –0.220 | –18.134 |
| N8 | –0.226 | –18.099 | N8 | –0.207 | –18.307 | N8 | –0.230 | –18.107 |
| N9 | –0.315 | –18.133 | N9 | –0.199 | –18.316 | N9 | –0.329 | –18.128 |
| N10 | –0.295 | –18.139 | N10 | –0.192 | –18.308 | N10 | –0.320 | –18.139 |
| N11 | –0.258 | –18.133 | N11 | –0.212 | –18.302 | N11 | –0.276 | –18.142 |
| N12 | –0.369 | –18.135 | N12 | –0.219 | –18.316 | N12 | –0.406 | –18.129 |
| B13 | 0.061 | –11.244 | B13 | 0.434 | –11.230 | B13 | 0.051 | –11.205 |
| N14 | –0.173 | –18.114 | N14 | –0.032 | –18.284 | N14 | –0.170 | –18.108 |
| N15 | -0.166 | –18.102 | N15 | –0.075 | –18.287 | N15 | –0.154 | –18.102 |

complexes. It is obvious that grabbing Cr, Mn, Fe, Zn, W, Cd by $B_5N_{10}$-nc might promote the strength of the nanocage that concludes an increase in the magnetic of clusters (Table2).

Figure5(a–f) indicated the same desire of shielding factor for boron and nitrogen; however, a remarkable deviation is observed from trapping atoms of Cr (16) (Figure5a), Mn (16) (Figure5b), Fe (16) (Figure5c), Zn (16) (Figure5d), W (16) (Figure5e), Cd (16) (Figure5f) through interaction with boron and nitrogen of $B_5N_{10}$-nc.

In Figure5 (a–f), toxic elements of Cr, Mn, Fe, Zn, W, Cd in the complexes of Cr↔$B_5N_{10}$-nc (Figure5a), Mn↔$B_5N_{10}$-nc (Figure5b), Fe↔$B_5N_{10}$-nc (Figure5c), Zn↔$B_5N_{10}$-nc (Figure5d), W↔$B_5N_{10}$-nc (Figure5e), and Cd↔$B_5N_{10}$-nc (Figure5f) describe the oscillation in the chemical shielding during atom capture.

Figure5 (a–f) defines the chemical shielding between boron/nitrogen in $B_5N_{10}$-nc and metal, metalloid and nonmetal atoms. Thus, it may be brought up that the turnover of electron admitting for the captured toxic atoms in the $B_5N_{10}$-nc is Cd> Zn> Fe> Mn > Cr≈ W that proves the strength of covalent bond across boron/nitrogen and these elements toward atom catching.

The curves of metal, metalloid and nonmetal elements of Cr, Mn, Fe, Zn, W, Cd through the trapping in the $B_5N_{10}$-nc during atom detection and removal from soil.

### 2.4. Interpreting Infrared (IR) Spectra

Trapping metal, metalloid and nonmetal elements of Cr, Mn, Fe, Zn, W, Cd in the $B_5N_{10}$-nc has been evaluated by IR spectroscopy during atom sensing in soil. The complexes of Cr↔$B_5N_{10}$-nc (Figure6a), Mn↔$B_5N_{10}$-nc (Figure6b), Fe↔$B_5N_{10}$-nc (Figure6c), Zn↔$B_5N_{10}$-nc (Figure6d), W↔$B_5N_{10}$-nc (Figure6e), and Cd↔$B_5N_{10}$-nc (Figure6f) have been analyzed through the IR spectroscopy.

The graph of Figure 6 (a) has been shown in the frequency about 200–1800 $cm^{-1}$ for Cr↔$B_5N_{10}$-nc with several sharp peaks around 655.26, 691.58, and 714.46$cm^{-1}$. Then, Figure 6 (b) was shown in the frequency limitation across 200–1100 $cm^{-1}$ for Mn↔$B_5N_{10}$-nc with several sharp peaks around 567.21, 616.88, 623.54, and 680.89 $cm^{-1}$. Figure 6 (c) has indicated the frequency around 1800–1100 $cm^{-1}$ for

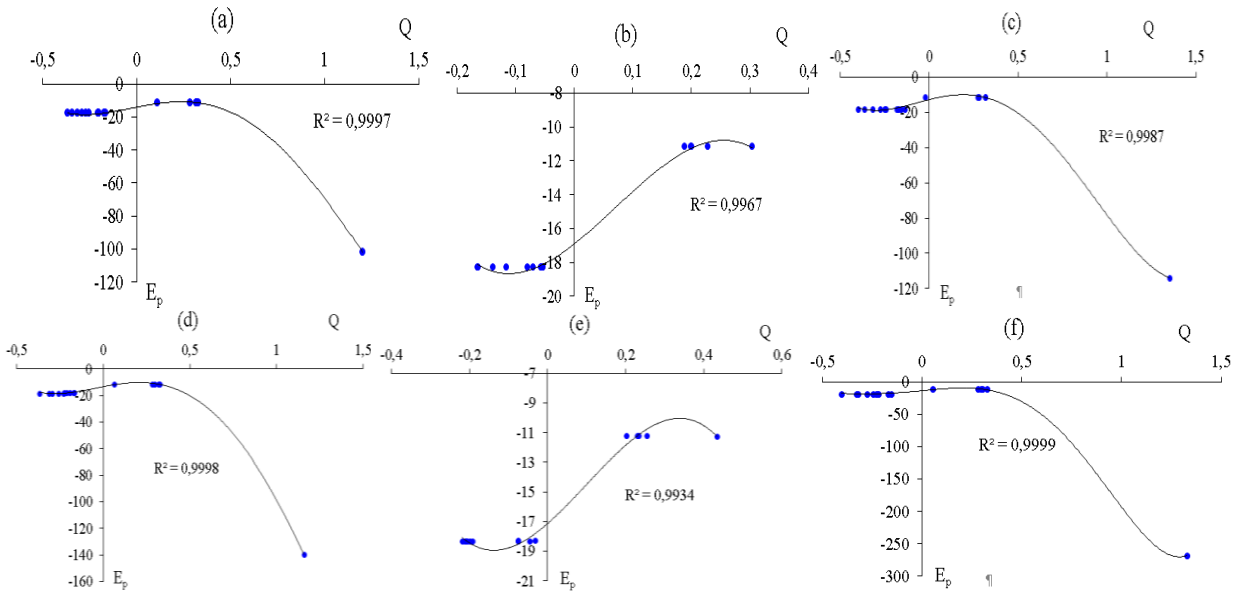


**Fig. 4.** The amounts of electric potential (Ep/a.u.) versus Bader charge (Q/coulomb) through NQR calculation for complexes of a) Cr↔$B_5N_{10}$-nc, b) Mn↔$B_5N_{10}$-nc, c) Fe↔$B_5N_{10}$-nc, d) Zn↔$B_5N_{10}$-nc, e) W↔$B_5N_{10}$-nc, and f) Cd↔$B_5N_{10}$-nc.

**Table2.**

Data of NMR shielding tensors for selected atoms of Cr↔$B_5N_{10}$-nc, Mn↔$B_5N_{10}$-nc, Fe↔$B_5N_{10}$-nc, Zn↔$B_5N_{10}$-nc, W↔$B_5N_{10}$-nc, and Cd↔$B_5N_{10}$-nc complexes using CAM–B3LYP–D3/LANL2DZ calculations.

| Cr ↔ $B_5N_{10}$-nc | | | Mn ↔ $B_5N_{10}$-nc | | | Fe ↔ $B_5N_{10}$-nc | | |
|---|---|---|---|---|---|---|---|---|
| Atom | $\sigma_{iso}$ | $\sigma_{aniso}$ | Atom | $\sigma_{iso}$ | $\sigma_{aniso}$ | Atom | $\sigma_{iso}$ | $\sigma_{aniso}$ |
| B1 | 117.007 | 83.0844 | B1 | 93.1958 | 74.3373 | B1 | 136.1640 | 112.1263 |
| N2 | 99.878 | 287.9554 | N2 | 107.1708 | 412.4542 | N2 | 252.7308 | 554.3353 |
| N3 | 38.330 | 429.4735 | N3 | 288.8404 | 780.6410 | N3 | 163.8389 | 480.5763 |
| B4 | 109.559 | 90.4106 | B4 | 98.4627 | 54.7623 | B4 | 137.8643 | 110.5202 |
| B5 | 104.411 | 97.3531 | B5 | 80.4756 | 75.4378 | B5 | 125.1732 | 101.4723 |
| B6 | 84.151 | 70.3800 | B6 | 80.8233 | 69.2619 | B6 | 137.0509 | 99.3871 |
| N7 | 65.830 | 250.6901 | N7 | 111.0482 | 258.3691 | N7 | 76.0677 | 523.9335 |
| N8 | 173.426 | 711.3619 | N8 | 359.3933 | 935.9902 | N8 | 5.1401 | 118.9943 |
| N9 | 228.262 | 477.9766 | N9 | 390.0925 | 580.1841 | N9 | 11.8325 | 408.4318 |
| N10 | 297.349 | 970.5455 | N10 | 353.0870 | 404.1981 | N10 | 15.6186 | 277.7235 |
| N11 | 112.155 | 469.8254 | N11 | 122.8970 | 484.1625 | N11 | 8.1861 | 651.2432 |
| N12 | 146.151 | 520.7535 | N12 | 126.0121 | 403.8011 | N12 | 40.8260 | 366.0072 |
| B13 | 23.4107 | 161.6682 | B13 | 51.7642 | 125.5008 | B13 | 92.9565 | 56.1805 |
| N14 | 61.4369 | 542.2817 | N14 | 390.1933 | 1289.4891 | N14 | 137.8765 | 620.3838 |
| N15 | 144.2153 | 582.4029 | N15 | 281.0691 | 1330.1789 | N15 | 66.2572 | 524.5995 |
| Cr16 | 8.8171 | 531.8666 | Mn16 | 4675.2397 | 3740.2405 | Fe16 | 982.3792 | 1080.9150 |
| Zn ↔ $B_5N_{10}$-nc | | | W ↔ $B_5N_{10}$-nc | | | Cd ↔ $B_5N_{10}$-nc | | |
| Atom | $\sigma_{iso}$ | $\sigma_{aniso}$ | Atom | $\sigma_{iso}$ | $\sigma_{aniso}$ | Atom | $\sigma_{iso}$ | $\sigma_{aniso}$ |
| B1 | 130.5100 | 91.8778 | B1 | 91.6888 | 68.8491 | B1 | 127.2884 | 98.7797 |
| N2 | 21.6821 | 546.0132 | N2 | 23.4058 | 244.5637 | N2 | 14.3171 | 555.9098 |
| N3 | 56.0171 | 57.5374 | N3 | 223.6585 | 505.2747 | N3 | 13.4107 | 122.4605 |
| B4 | 120.3790 | 53.0462 | B4 | 92.2361 | 72.9567 | B4 | 103.1204 | 115.3330 |
| B5 | 115.0078 | 68.5589 | B5 | 81.6149 | 72.3481 | B5 | 118.2561 | 61.9536 |
| B6 | 133.6303 | 81.2506 | B6 | 79.3710 | 80.4153 | B6 | 123.6742 | 80.8870 |
| N7 | 1.3263 | 478.3851 | N7 | 67.1424 | 230.3649 | N7 | 131.6130 | 549.6007 |
| N8 | 51.1373 | 184.3061 | N8 | 331.0739 | 856.4636 | N8 | 19.8739 | 130.0665 |
| N9 | 134.4198 | 330.9866 | N9 | 454.0576 | 614.2209 | N9 | 97.3508 | 203.8768 |
| N10 | 55.0733 | 270.0957 | N10 | 432.1887 | 652.7413 | N10 | 41.2612 | 585.3871 |
| N11 | 35.5475 | 334.9535 | N11 | 276.3243 | 480.2979 | N11 | 26.8124 | 253.2975 |
| N12 | 166.1786 | 238.3185 | N12 | 133.3741 | 462.9130 | N12 | 25.7318 | 620.6356 |
| B13 | 126.7224 | 17.4660 | B13 | 17.5072 | 225.2369 | B13 | 139.3014 | 55.8459 |
| N14 | 32.3937 | 478.1249 | N14 | 413.1482 | 983.4193 | N14 | 47.7721 | 423.7621 |
| N15 | 104.9527 | 596.0890 | N15 | 381.9037 | 1002.6071 | N15 | 92.9321 | 392.1182 |
| Zn16 | 2920.2381 | 3680.6586 | W16 | 37.9252 | 77.2940 | Cd16 | 3945.3535 | 242.5438 |

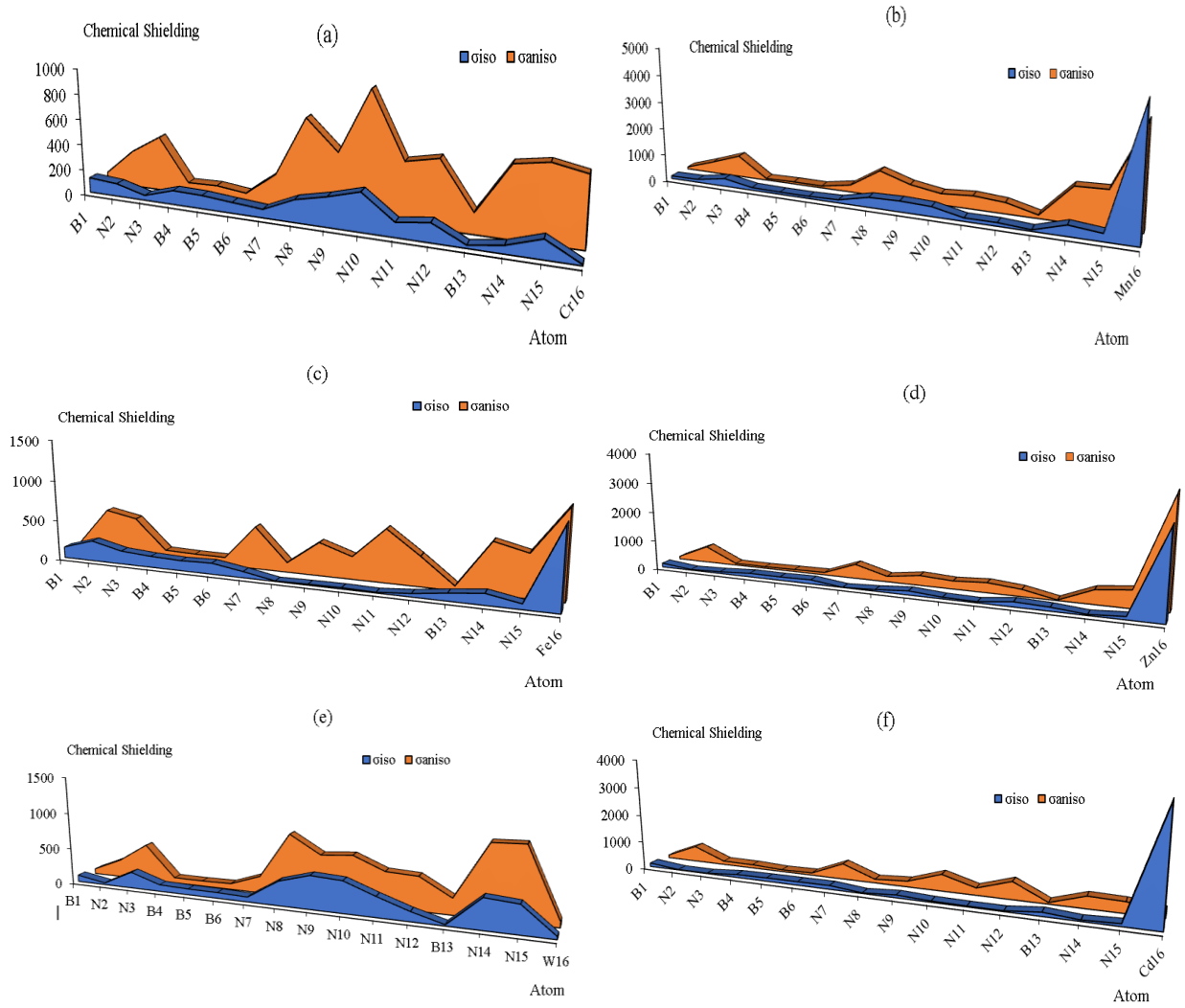


**Fig. 5.** The NMR spectrum for complexes of a) Cr↔$B_5N_{10}$-nc, b) Mn↔$B_5N_{10}$-nc, c) Fe↔$B_5N_{10}$-nc, d) Zn↔$B_5N_{10}$-nc, e) W↔$B_5N_{10}$-nc, and f) Cd↔$B_5N_{10}$-nc using CAM–B3LYP–D3/LANL2DZ.

Fe↔$B_5N_{10}$-nc with one sharp peak around 983.42 $cm^{-1}$. Figure 6 (d) has shown the fluctuation frequency between 50–950 $cm^{-1}$ for Zn↔$B_5N_{10}$-nc with two sharp peaks around 537.66 and 902.68 $cm^{-1}$. Figure6 (e) has indicated the fluctuation of frequency between 200–1400 $cm^{-1}$ for W↔$B_5N_{10}$-nc with several sharp peaks around 582.28, 656.11, 664.63, 723.76, and 798.39 $cm^{-1}$. Figure6 (f) has shown the frequency range between 100–1600 $cm^{-1}$ for Cd↔$B_5N_{10}$-nc with several sharp peaks around 504.75, 1002.32, and 1233.14$cm^{-1}$. Table 3 has described that $B_5N_{10}$-nc owing to capture transition metals including Cr, Mn, Fe, Zn, W, Cd might be more efficient detector for sensing and catching these elements from soil.

Table 3 could introduce the ability of metal, metalloid and nonmetal elements of Cr, Mn, Fe, Zn, W, Cd trapped in the $B_5N_{10}$-nc through $\Delta G^{o}_{ads}$ which is related to the covalent bond between these elements and $B_5N_{10}$-nc as a potent detector for soil purification.

The trapping process of metal, metalloid and nonmetal elements including Cr, Mn, Fe, Zn, W, Cd in the $B_5N_{10}$-nc is affirmed by the $\Delta G^{o}_{ads}$ quantities:

$$\Delta G^{o}_{ads} = \Delta G^{o}_{X\leftrightarrow B5N10-nc} - \left(\Delta G^{o}_{X-grabbed} + \Delta G^{o}_{B5N10-nc}\right); \quad X= Cr, Mn, Fe, Zn, W, Cd \qquad (10).$$

Furthermore, Table 3 has shown that the dependence on the size of the atoms of during interaction between the adsorbates of the metal, metalloid and nonmetal elements as the electron acceptors and the adsorbent of $B_5N_{10}$-nc as electron donor in the complexes of Cr↔$B_5N_{10}$-nc, Mn↔$B_5N_{10}$-nc, Fe↔$B_5N_{10}$-nc, Zn↔$B_5N_{10}$-nc, W↔$B_5N_{10}$-nc, and Cd↔$B_5N_{10}$-nc. Therefore, the selectivity of the metal, metalloid and nonmetal elements by $B_5N_{10}$-nc (atom sensor) can be resulted as:
Cd> Zn> Fe> Cr> Mn ≈ W (Table 3).

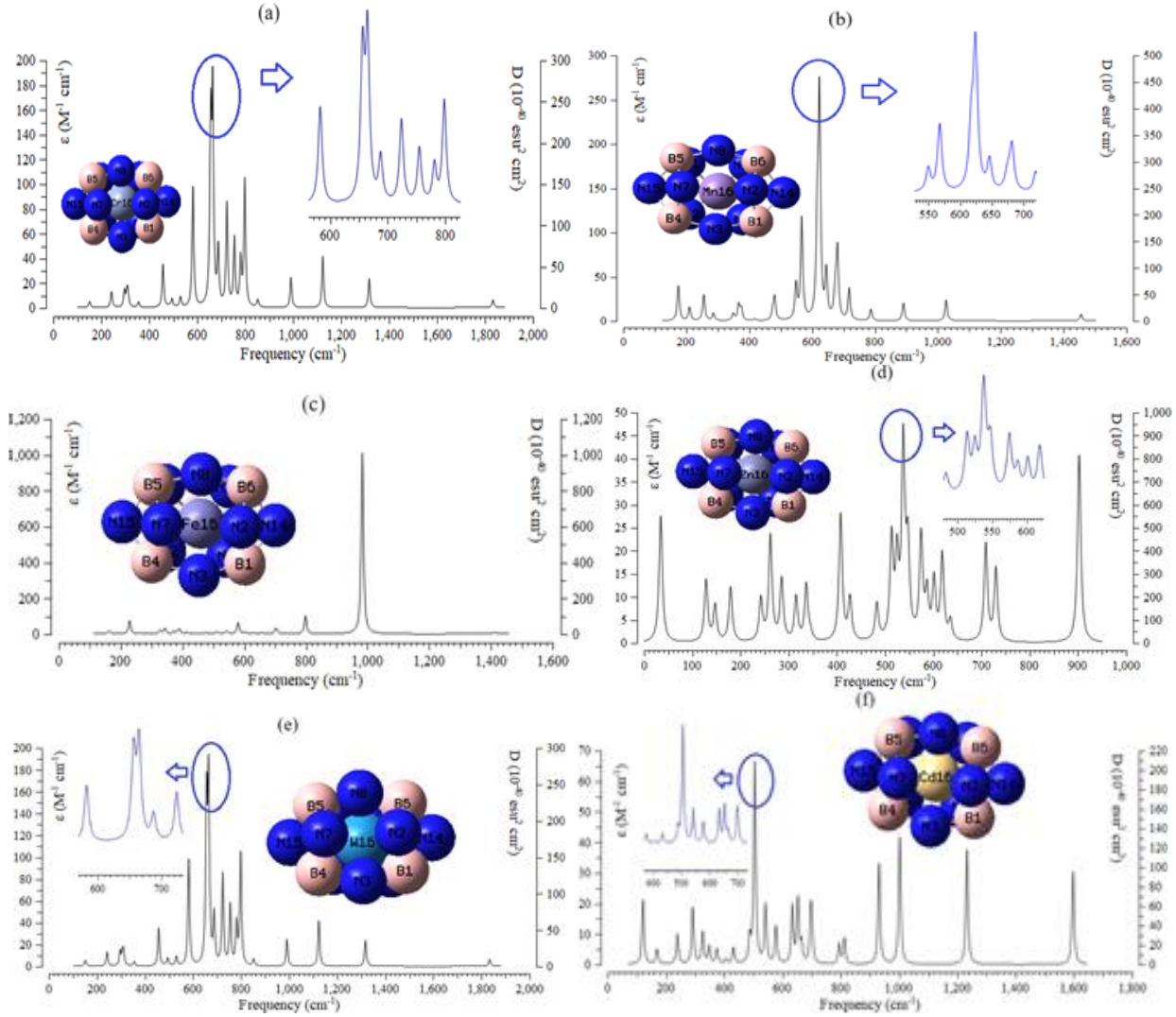


**Fig. 6.** IR spectra for complexes of a) Cr↔$B_5N_{10}$-nc, b) Mn↔$B_5N_{10}$-nc, c) Fe↔$B_5N_{10}$-nc, d) Zn↔$B_5N_{10}$-nc, e) W↔$B_5N_{10}$-nc, and f) Cd↔$B_5N_{10}$-nc complexes.

**Table3.**

The thermochemical characters of Cr↔$B_5N_{10}$-nc, Mn↔ $B_5N_{10}$-nc, Fe↔ $B_5N_{10}$-nc, Zn↔$B_5N_{10}$-nc, W↔$B_5N_{10}$-nc, and Cd↔$B_5N_{10}$-nc complexes.

| Compound | Dipole moment (Debye) | $\Delta E^o \times 10^{-3}$ (kcal/mol) | $\Delta H^o \times 10^{-3}$ (kcal/mol) | $\Delta G^o \times 10^{-3}$ (kcal/mol) | $S^o$ (cal/K.mol) |
|---|---|---|---|---|---|
| $B_5N_{10}$-nc | 0.202 | –420.550 | –420.549 | –420.579 | 100.650 |
| Cr↔$B_5N_{10}$-nc | 0.694 | –1063.754 | –1063.754 | –1063.782 | 94.375 |
| Mn↔$B_5N_{10}$-nc | 0.489 | –485.602 | –485.602 | –485.629 | 90.852 |
| Fe↔$B_5N_{10}$-nc | 1.448 | –1199.586 | –1199.585 | –1199.614 | 95.351 |
| Zn↔$B_5N_{10}$-nc | 0.941 | –1518.749 | –1518.748 | –1518.780 | 105.321 |
| W↔$B_5N_{10}$-nc | 0.594 | –462.747 | –462.746 | –462.774 | 90.867 |
| Cd↔$B_5N_{10}$-nc | 0.756 | –3811.957 | –3811.957 | –3811.985 | 93.836 |

## Conclusion

$B_5N_{10}$-nc can be used to capture metal, metalloid and nonmetal elements from soil because of electrostatic interactions between metal, metalloid and nonmetal elements and $B_5N_{10}$-nc. The thermochemistry and electromagnetic parameters of Cr, Mn, Fe, Zn, W, Cd absorbed $B_5N_{10}$-nc have been illustrated by DFT method. The consequences have defined that Cr, Mn, Fe, Zn, W, Cd trapped in $B_5N_{10}$-nc are rather fixed with the most stable adsorption site being in the center of $B_5N_{10}$-nc system. Catching Cr, Mn, Fe, Zn, W, Cd in the $B_5N_{10}$-nc happens due to chemisorption phenomenon. The n-grabbing behavior can be found in $B_5N_{10}$-nc after the adsorption of Cr, Mn, Fe, Zn, W, Cd. The work function of $B_5N_{10}$-nc has remarkably exhibited the transition metals adsorption with maximum amount for the
Cd> Zn> Fe> Cr> Mn ≈ W –adsorbed $B_5N_{10}$-nc system.

Moreover, it is proposed that transition metals-adsorbed can be employed to design and progress the

optoelectronic specification of $B_5N_{10}$-nc for inventing photoelectric instruments.

***Fatemeh Mollaamin*** – Ph.D. degree of Physical Chemistry in the field of Quantum Chemistry, Professor, University Faculty Member.

**Acknowledgements**

*In successfully completing this paper and its research, the author is grateful to Kastamonu University.*

[1] Changfeng Li, et el., *A Review on Heavy Metals Contamination in Soil: Effects, Sources, and Remediation Techniques.* Soil and Sediment Contamination: An International Journal, 28 (4), 380 (2019); https://doi.org/10.1080/15320383.2019.1592108.

[2] Z. He, et el., *Heavy Metal Contamination of Soils: Sources, Indicators, and Assessment*, Journal of Environmental Indicators, 9, 17 (2015).

[3] *risk assessment of mercury in kindergarten dust*. Atmos. Environ. 73, 169 (2013); https://doi.org/10.1016/j.atmosenv.2013.03.017.

[4] G.Y. Sun, et el., *Geochemical assessment of agricultural soil: A case study in Songnen-Plain (Northeastern China).* Catena, 111, 56 (2013);. https://doi.org/10.1016/j.catena.2013.06.026.

[5] O. Morton-Bermea, et el., *Assessment of heavy metal pollution in urban topsoils from the metropolitan area of Mexico City*. J. Geochem. Explor. 101, 218(2009); https://doi.org/10.1016/j.gexplo.2008.07.002.

[6] K. Ji, et al. *Assessment of exposure to heavy metals and health risks among residents near abandoned metal mines in Goseong, Korea*. Environ. Pollut. 178, 322 (2013); https://doi.org/10.1016/j.envpol.2013.03.031.

[7] S. Kim, et el., *The effect of exposure factors on the concentration of heavy metals in residents near abandoned metal mines*. J. Prev. Med. Public Health, *44*, 41(2011); https://doi.org/10.3961/jpmph.2011.44.1.41.

[8] G.V. Motuzova, et el., *Soil contamination with heavy metals as a potential and real risk to the environment*, Journal of Geochemical Exploration, 144, Part B, 241 (2014); https://doi.org/10.1016/j.gexplo.2014.01.026.

[9] N.H. Al-Makishah, M.A. Taleb, & M.A. Barakat, *Arsenic bioaccumulation in arsenic-contaminated soil: a review*. Chem. Pap., 74, 2743 (2020); https://doi.org/10.1007/s11696-020-01122-4.

[10] Giovana Poggere, et el., *Soil contamination by copper: Sources, ecological risks, and mitigation strategies in Brazil,* Journal of Trace Elements and Minerals, 4, 100059 (2023); https://doi.org/10.1016/j.jtemin.2023.100059.

[11] Miao Jiang, et el., *Technologies for the cobalt-contaminated soil remediation: A review,* Science of The Total Environment, 813, 151908 (2022); https://doi.org/10.1016/j.scitotenv.2021.151908.

[12] Evandro B. da Silva, et el., *Background concentrations of trace metals As, Ba, Cd, Co, Cu, Ni, Pb, Se, and Zn in 214 Florida urban soils: Different cities and land uses*, Environmental Pollution, 264, 114737 (2010); https://doi.org/10.1016/j.envpol.2020.114737.

[13] F. Mollaamin, *Features of parametric point nuclear magnetic resonance of metals implantation on boron nitride nanotube by density functional theory/electron paramagnetic resonance*. Journal of Computational and Theoretical Nanoscience, 11(11), 2393 (2014); https://doi.org/10.1166/jctn.2014.3653.

[14] F. Mollaamin, et el., *Computational Modelling of Boron Nitride Nanosheet for Detecting and Trapping of Water Contaminant.* Russ. J. Phys. Chem. B, 18, 67 (2024); https://doi.org/10.1134/S1990793124010330.

[15] R.S. Bangari, et el., *$Fe_3O_4$-functionalized boron nitride nanosheets as novel adsorbents for removal of arsenic(III) from contaminated water*. ACS Omega, 5 (18) 10301 (2020); https://doi.org/10.1021/acsomega.9b04295.

[16] G. Henkelman, A. Arnaldsson, and H Jónsson, *A fast and robust algorithm for Bader decomposition of charge density*, Computational Materials Science 36(3), 354(2006); https://doi.org/10.1016/j.commatsci.2005.04.010.

[17] J.P. Perdew, K. Burke, M. Ernzerhof, *Generalized gradient approximation made simple*. Phys. Rev. Lett., 77, 3865 (1996); https://doi.org/10.1103/PhysRevLett.77.3865.

[18] W. Kohn, L. J. Sham, *Self-Consistent Equations Including Exchange and Correlation Effects*. Phys. Rev., 140, A1133(1965); https://doi.org/10.1103/PhysRev.140.A1133.

[19] C. Lee, W. Yang, R.G. Parr, *Development of the Colle–Salvetti correlation-energy formula into a functional of the electron density*. Phys Rev B, 37,785 (1988); https://doi.org/10.1103/PhysRevB.37.785.

[20] Takeshi Yanai, David P Tew, Nicholas C Handy, *A new hybrid exchange–correlation functional using the Coulomb-attenuating method (CAM-B3LYP*), Chemical Physics Letters, 393 (1–3), 51 (2004); https://doi.org/10.1016/j.cplett.2004.06.011.

[21] S. Grimme, J. Antony, S. Ehrlich, H. Krieg, A consistent and accurate ab initio parametrization of density functional dispersion correction (DFT-D) for the 94 elements H-Pu, J Chem Phys. 132(15),154104 (2010); https://doi.org/10.1063/1.3382344.

[22] S. Grimme, S. Ehrlich, L. Goerigk, *Effect of the damping function in dispersion corrected density functional theory*. J Comput Chem, 32(7), 1456 (2011); https://doi.org/10.1002/jcc.21759.

[23] M.J. Frisch, et al. Gaussian 16, Revision C.01, Gaussian, Inc., Wallingford CT, 2016.

[24] Dennington, Roy; Keith, Todd A.; Millam, John M., GaussView, Version 6.06.16, Semichem Inc., Shawnee Mission, KS, (2016).

[25] V.K. Ahluwalia, *Nuclear Quadrupole Resonance (NQR) Spectroscopy. In: Instrumental Methods of Chemical Analysis*. Springer, Cham. (2023); https://doi.org/10.1007/978-3-031-38355-7_30.
[26] Young, Hugh A., Freedman, Roger D. *Sears and* Zemansky's University Physics with Modern Physics (13th ed.). Boston: Addison-Wesley. 754, (2012);
[27] I.P. Gerothanassis, T. Kupka, *New Insights into Nuclear Magnetic Resonance (NMR) Spectroscopy*. Molecules, 30, 1500 (2025); https://doi.org/10.3390/molecules30071500.
[28] M.T. Caccamo, et el., *Infrared spectroscopy analysis of montmorillonite thermal effects*. IOP Conf. Ser.: Mater. Sci. Eng. 777, 012002 (2020); https://doi.org/10.1088/1757-899X/777/1/012002.

Фатеме Меламін

# Наноматеріали для екологічної ремедіації ґрунтів шляхом вилучення токсичних перехідних металів: структурний, електромагнітний та термодинамічний аналіз з використанням DFT

*Кафедра біомедичної інженерії, Інженерно-архітектурний факультет, Університет Кастамону, Кастамону, Туреччина, fmollaamin@kastamonu.edu.tr*

Метою дослідження є видалення з ґрунту перехідних металів Cr, Mn, Fe, Zn, W, Cd з використанням наноматеріалу на основі нітриду галію — наноклітки $B_5N_{10}$ ($B_5N_{10}$-nc). Електромагнітні та термодинамічні характеристики токсичних перехідних металів, захоплених у $B_5N_{10}$-nc, описано за допомогою методів комп'ютерного моделювання матеріалів. Досліджено поведінку процесу захоплення іонів Cr, Mn, Fe, Zn, W, Cd нанокліткою $B_5N_{10}$-nc з метою сенсорного виявлення катіонів металів у ґрунті. Структуру $B_5N_{10}$-nc було змодельовано у присутності перехідних металів (Cr, Mn, Fe, Zn, W, Cd), а характеризацію систем проведено методом теорії функціонала густини (DFT). Ковалентна природа зв'язків у відповідних комплексах продемонструвала подібність енергетичних рівнів і характер часткової густини електронних станів між p-станами бору та азоту у $B_5N_{10}$-nc і d-станами Cr, Mn, Fe, Zn, W, Cd у комплексах X↔$B_5N_{10}$-nc. Крім того, аналіз ядерного магнітного резонансу (ЯМР) виявив виражені піки навколо атомів Cr, Mn, Fe, Zn, W, Cd у процесі їх захоплення $B_5N_{10}$-nc під час детектування та вилучення з ґрунту; водночас спостерігаються певні флуктуації у хімічному екрануванні ізотропних та анізотропних тензорів. На основі отриманих результатів встановлено селективність адсорбції токсичних металів, металоїдів і неметалів нанокліткою $B_5N_{10}$-nc (атомний сенсор) у такому порядку: Cd > Zn > Fe > Cr > Mn ≈ W**.** У роботі запропоновано використовувати системи з адсорбованими токсичними металами, металоїдами та неметалами для проєктування та розширення оптоелектронних характеристик $B_5N_{10}$-nc з метою створення фотоелектричних приладів для очищення ґрунтів.

**Ключові слова:** забруднення ґрунтів, $B_5N_{10}$-nc, молекулярне моделювання, наноматеріал, DFT.